Main-Ion Intrinsic Toroidal Rotation Profile Driven by Residual Stress Torque from Ion Temperature Gradient Turbulence in the DIII-D Tokamak

B. A. Grierson, W. X. Wang, S. Ethier, G. M. Staebler, D. J. Battaglia, J. A. Boedo, J. S. deGrassie, and W. M. Solomon

Phys. Rev. Lett. **118**, 015002 — Published 6 January 2017

DOI: 10.1103/PhysRevLett.118.015002

Main-ion intrinsic toroidal rotation profile driven by residual stress torque from ion temperature gradient turbulence in the DIII-D tokamak

B. A. Grierson,[1,*] W.X. Wang,[1] S. Ethier,[1] G.M. Staebler,[2] D.J. Battaglia,[1] J.A. Boedo,[3] J.S. deGrassie,[2] and W.M. Solomon[2]

[1]*Princeton Plasma Physics Laboratory, Princeton University, Princeton, NJ 08543, USA*
[2]*General Atomics, P.O. Box 85608, San Diego, CA 92186-5608*
[3]*Center for Energy Research, University of California San Diego, 9500 Gilman Dr., La Jolla, CA 92093-0417*

(Dated: December 9, 2016)

Intrinsic toroidal rotation of the deuterium main-ions in the core of the DIII-D tokamak is observed to transition from flat to hollow, forming an off-axis peak, above a threshold level of direct electron heating. Nonlinear gyrokinetic simulations show that the residual stress associated with electrostatic ITG turbulence possesses the correct radial location and stress structure to cause the observed hollow rotation profile. Residual stress momentum flux in the gyrokinetic simulations is balanced by turbulent momentum diffusion, with negligible contributions from turbulent pinch. Prediction of the velocity profile by integrating the momentum balance equation produces a rotation profile that qualitatively and quantitatively agrees with the measured main-ion profile, demonstrating that fluctuation-induced residual stress can drive the observed intrinsic velocity profile.

PACS numbers: 52.30.-q,52.25.Fi,52.35.Ra,52.65.Tt

Introduction— Turbulent transport in fluid systems such as Earth's atmosphere, stellar and laboratory plasmas can produce striking, self-organized features in the energy, density and momentum[1, 2] of the medium. In a tokamak, the phenomena of self-organized angular momentum creates an "intrinsic" rotation, where differential fluid flow can arise spontaneously. Intrinsic rotation here is defined by the magnitude and shape of the toroidal angular velocity profile that self-organizes in the absence of auxiliary torque injection, and can exhibit a wide range of nonlinear phenomenology[3] including threshold behavior across subtle changes in plasma conditions, as well as bifurcations in the rotation direction[4, 5]. This plasma rotation is well known to have beneficial effects on energy confinement[6] and plasma stability[7]. In future large tokamaks such as ITER the rotation profile of the main-ions is expected to be largely determined by intrinsic processes because the ability of auxiliary torque to drive plasma rotation will be much smaller than in existing devices. ITER will operate in a regime that is dominantly electron heated by fusion alpha particles, where the heating of the ions will be dominantly through collisional energy exchange, motivating intrinsic rotation studies and model validation with direct electron heating and nearly equilibrated electron and ion temperatures. These considerations motivate achieving a validated predictive capability for main-ion intrinsic toroidal rotation for projection to ITER.

In this Letter we report the first measurement of main-ion (deuterium) intrinsic toroidal rotation undergoing a profile inversion, whereby an initially flat, slightly positive rotation profile reverses direction (Fig. 1) and becomes hollow. The hollow rotation profile is quantitatively predicted by global nonlinear gyrokinetic simulations. This observation is made in deuterium plasmas with direct electron heating and nearly equilibrated electron and ion temperature profiles. Above a critical heating power the plasma becomes linearly unstable to ion temperature gradient driven turbulence. Global nonlinear simulations with `GTS`[8] confirm a residual stress in the unstable region. Ion temperature gradient (ITG) turbulence produces a negative intrinsic torque at inner radii, driving the rotation profile in the direction opposite to the plasma current, and a positive torque at outer radii, driving the plasma in the same direction as the plasma current. The intrinsic torque is balanced by turbulent diffusion producing a local positive rotation gradient, or hollow profile, in the absence of auxiliary torque. Gyrokinetic calculations of the fluctuation-induced residual stress and resulting main-ion toroidal velocity profile that produces the zero-flux state are shown to be consistent with both the shape and magnitude of the observed rotation profile.

Previous investigations of similar rotation phenomena have been reported in ohmic plasmas whereby the entire plasma column changes sign from co-current to counter-current during controlled increases in the plasma density[5], and well documented core rotation reversals during transitions from linear ohmic to saturated ohmic confinement regimes identifying plasma collisionality as the strongest correlation [4, 9]. In helium main-ion plasmas on DIII-D the radial location of the helium velocity hollowing was seen to be dependent on the deposition location of the electron heating[10, 11], which ties the

reversal phenomenon to the energy flux. Variations of the rotation gradient with changes of the local density gradient have been also been observed[12] indicating the need for local profile investigation to organize the observations. Investigations into the type of linearly unstable turbulence between ion and electron modes that correlate with the observations have been explored [12–14], indicating that other processes beyond the dominant turbulence mode, such as the collisionality scaling of non-Maxwellian equilibria[15], are required to explain the wide range of observed phenomenology. The results in this Letter with global nonlinear gyrokinetic simulations using experimental profiles show that the intrinsic torque from ITG has the correct spatial location, structure and magnitude to produce the experimentally observed main-ion intrinsic rotation profiles under the conditions reported in the following section.

Experiment— Core main-ion [16, 17] toroidal rotation reversal is obtained during an increase of direct electron heating from 0.5 to 1.0 MW that raises the temperature of both electrons and ions. Experiments were carried out on the DIII-D tokamak[18] in low confinement mode (L-mode) heated by electron cyclotron waves at the second harmonic frequency positioned near the plasma half-radius. Discharges are formed with an upper-single-null shape with the magnetic field drift direction away from the active X-point and operated with $q_{95} \approx 5.5$. In these L-mode plasmas the concentration of carbon impurity is between $1.0 - 1.2\%$ such that the momentum is carried by the main-ions. Line-averaged density near $2.5 - 3 \times 10^{19}\ m^{-3}$ is sufficient for collisional coupling of electron and ion species such that electron cyclotron resonance heating raises both electron and ion temperatures due to collisional energy exchange, seen in Fig. 2(a,b). Therefore direct electron heating in these plasmas increases both electron and ion pressure gradients that can drive instabilities. However, inside of $\rho = 0.5$ the plasma is heated ohmically, and produces low levels of ion energy flux that are near the neoclassical level. Upon increasing the heating power from 0.5 to 1.0 MW the power flow from the electrons through the ion channel increases above the neoclassical levels. The electron density profile (Fig. 2(c)) shows a smaller variation between 0.5 to 1.0 MW than the temperature profiles, and the increase of the temperature reduces the collisionality as the rotation profile hollows. Through a sequential increase in the electron heating from 0.5, 1.0, 1.7 and 2.2 MW we discover a reversal of the core deuterium toroidal velocity between 0.5 and 1.0 MW, displayed in Fig. 1. Here the main-ion toroidal velocity profile is measured [16, 17] by short neutral beam pulses spaced approximately one second (many momentum confinement times) apart. The momentum injection on the measurement timescale is negligible. For heating powers of 1.0 MW and above the profiles are resilient to change, the energy confinement variation with power transitions from flat to decreasing, (Fig. 2(d)), and the rotation profile maintains the hollow state seen in Fig. 1.

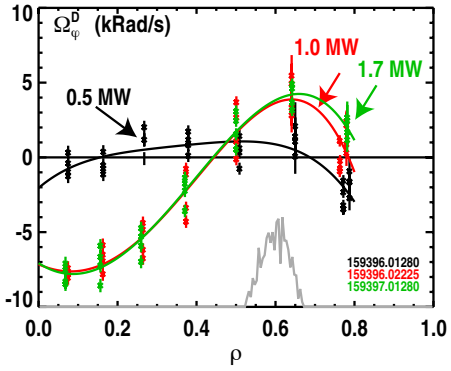

FIG. 1: Experimental main-ion toroidal rotation profiles displaying a reversed rotation profile upon increasing the heating power from 0.5, 1.0, 1.7 MW ECH.

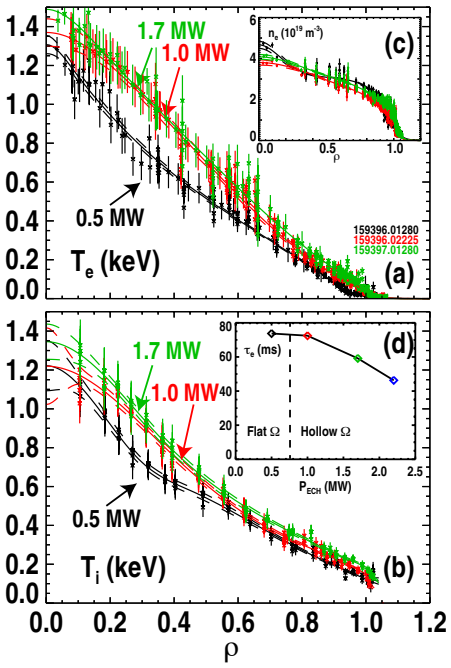

FIG. 2: Experimental (a) electron and (b) ion temperature profiles and (c) electron density profiles for 0.5, 1.0 and 1.7 MW of ECH. Above 1.0 MW of ECH the profiles are resilient to changes and the energy confinement (d) degrades.

Theory— Intrinsic rotation arises due to an intrinsic torque caused by turbulence in the presence of various effects that break the structure symmetry in the gyrokinetic equation[19–21] , and the fluctuation symmetry in the parallel wavenumber spectrum[22, 23]. Physics mechanisms that may cause the broken symmetries, and thus the generation of residual Reynolds stress include finite shear in the $\mathbf{E} \times \mathbf{B}$ velocity[24, 25], up/down asymmetry in equilibrium geometry[26], radial gradient in the turbulence intensity[27], poloidal tilt of global mode struc-

ture arising from the profile shearing [28], and magnetic shear effects on turbulence spectrum [29]. Higher order terms in the gyrokinetic equation are also being investigated for further symmetry breaking mechanisms in nonlinear gyrokinetics[20]. An underlying turbulent fluctuation at the ion scale in the low wavenumber range $k_\theta \rho_s \leq 1$ is required to cause momentum transport carried by the main-ions because the ion response to high-k fluctuations is nearly adiabatic. Linear turbulence stability shows that at mid-radius $\rho \approx 0.4 - 0.6$ prior to increased auxiliary heating the low-k growth rates are stable, whereas after 1.0 MW of electron heating is applied the ion temperature profile becomes linearly unstable to long-wavelength ITG modes. Linear stability was tested with Monte-Carlo random error analysis of a/L_{Ti} for the ion temperature profile at 0.5 MW shown in Fig. 2(b), which is linearly stable within the error estimates. Displayed in Fig. 3 are the linear growth rate and frequency spectra from the TGLF model[30] based on measured plasma profiles including impurities, indicating that a threshold in ITG stability has been crossed by the additional heating. The lack of linearly unstable modes in Fig. 3(a) results in underdeveloped turbulence that produces little turbulent flux or residual stress. This is consistent with experimental observations that the ion energy transport is near neoclassical levels, the turbulent intrinsic torque produced in the low power phase should be small, and other effects such as neoclassical transport remain to be studied in the low power phase.

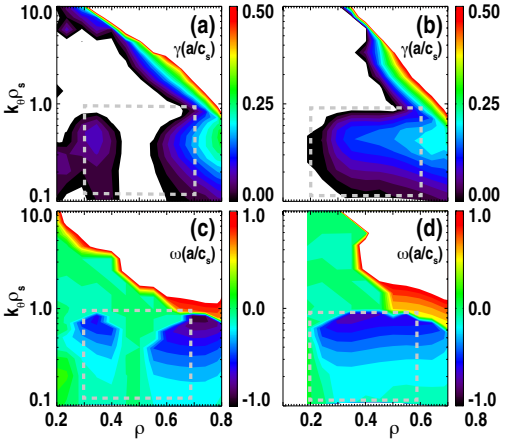

FIG. 3: Linear turbulence stability at displaying excitation of linearly unstable ITG turbulence upon power step from 0.5 MW (a) to 1.0 MW (b) with appearance of mid-radius finite growth rate with negative frequency (c,d). Box indicates growth rate (a,b) and frequency (b,c) at low wavenumber $k_\theta \rho_s < 1.0$.

In order to compute the turbulent fluxes associated with linearly unstable ITG modes in Fig. 3(b), we use the gradient-driven δf global nonlinear gyrokinetic simulation GTS[8] that evolves an initially Maxwellian plasma with profiles and equilibrium radial electric field taken directly from the experiment without adjustment. GTS used for this study focuses on global turbulence effects and the effect of up-down geometric asymmetry for the symmetry breaking needed for turbulence-driven toroidal momentum flux. Such global effects have been proven to be significant for turbulence to drive residual stress in many previous gyrokinetic studies. The higher order terms in the gyrokinetic equation, which are needed to break the gyrokinetic structure symmetry in the local flux-tube limit, are not included here.

Simulations are electrostatic with kinetic electrons over the wavenumber range $k_\theta \rho_s \leq 2$, which covers the relevant low-k modes shown in Fig. 3. Numerical equilibrium from EFIT reconstruction including MSE polarimetry extracted from TRANSP[31] is used, and the simulations are executed in a manner similar to Ref. [32]. Simulations are run well beyond the linear growth phase of the instability to reach a well-saturated, stationary turbulence state. As is generally done for calculating transport fluxes in this type of turbulence simulation study, a steady-state momentum flux profile is obtained by time average in the saturated turbulence state over a long period. Generally, the interval of time averaging should be some time scale between the correlation time and the profile evolution time. More specifically, an averaged transport flux is calculated over a period of many turbulence growth times.

Interpretation of rotation and momentum transport is guided by casting the total toroidal Reynolds stress in terms of diffusive, pinch and residual fluxes (Eq. 1), which have been studied experimentally on DIII-D[33].

$$\Pi_\varphi = -m_i n_i \langle R^2 |\nabla\rho| \rangle \left(\chi_\varphi \frac{d\Omega_\varphi}{d\rho} - V_p \Omega_\varphi \right) + \Pi^{resid.} \quad (1)$$

where ρ denotes flux surfaces, Ω is the main-ion toroidal angular rotation frequency, χ_φ is the momentum diffusivity, V_p is the pinch velocity, $\Pi^{resid.}$ is the residual stress and the other terms are of standard usage. In steady-state the total toroidal momentum flux must be equal to zero in the absence of external toroidal torque. The balance of three terms plus the boundary condition will determine the toroidal rotation profile. By global nonlinear gyrokinetic simulation the residual stress component $\Pi^{resid.}$ of the total stress is directly calculated by zeroing the velocity-dependent contributions ($\Omega_\varphi = 0, d\Omega_\varphi/d\rho = 0$), and is displayed in Fig. 4 in units described in Ref. [8]. Over the time period of 400-700 (v_{th}/L_{Ti}) the structure and magnitude of the stress is saturated and is taken as stationary. This residual stress depends on the background profiles and gradients of the plasma density and temperature, geometry and quantities derived therefrom. In the case of small Mach number and low parallel velocity shear, which is satisfied in these experimental conditions, the linear stability and turbulent fluxes do not depend on the velocity profile. Qualitatively, the dipolar structure of the residual stress in Fig. 4 has the capability

to produce a hollow intrinsic rotation profile because the associated positive intrinsic momentum flux for $\rho < 0.6$ and negative momentum flux at $\rho > 0.6$ balance against momentum diffusion.

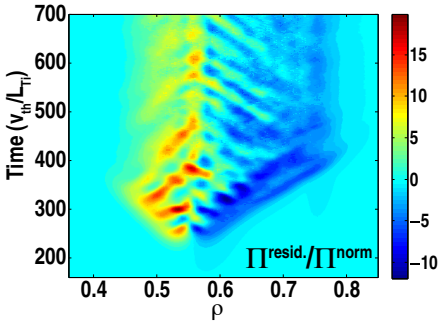

FIG. 4: Residual stress displaying dipolar structure that produces the hollow rotation profile.

Profile Prediction—Making an *ab initio* quantitative prediction of the intrinsic rotation requires a residual stress, momentum diffusivity, pinch velocity and boundary condition. The residual stress computed in the previous section and radial electric field are held fixed as we next compute the diffusion and pinch contributions to the momentum flux with two more GTS simulations. As the rotation profile itself would not be available in an *ab initio* prediction to compute χ_φ, we use the ratio of the ion momentum diffusivity to ion heat diffusivity Prandtl number $Pr \equiv \chi_\varphi/\chi_i$, whose value is well established both theoretically and experimentally to be near unity[19, 34]. The chosen Prandtl number in our model is not arbitrary, but is confirmed by nonlinear gyrokinetic simulations to be near the expected value of $Pr = 0.7$, consistent with previous studies[19, 35]. Fig. 5 shows the radial profile of the ion heat diffusivity and momentum diffusivity computed by GTS for this DIII-D discharge. In the region where the rotation gradient is not close to zero and χ_φ is well defined, the simulated momentum diffusivity is less than the thermal diffusivity, and the Prandtl number, on a profile average, is $Pr \approx 0.7$. Using the Prandtl number enables us to use χ_i that is obtained directly from the gyrokinetic simulation, instead of χ_φ directly, in the prediction. Power balance analysis with TRANSP[31] indicates that the experimental χ_i is 0.5-1.5 m^2/s near $\rho = 0.6$, which contains the value produced by GTS. The momentum pinch velocity is found to be negligible for these conditions, which is verified by including a finite, zero gradient rotation profile in a dedicated gyrokinetic simulation and comparing the residual stress momentum flux to the total momentum flux. As can be seen in Fig. 6 the momentum pinch makes a negligible contribution to the momentum balance and the diffusive momentum flux produced from the measured rotation profile approximately balances the residual stress.

Having obtained all components of the toroidal momentum balance equation, a first-principles-based main-ion intrinsic toroidal rotation profile is obtained by setting $\Pi_\varphi \equiv 0$ in Eq. 1 numerically integrating for $\Omega_\varphi(\rho)$, determining the toroidal rotation profile within a constant. Displayed in Fig. 7(a,b) are the experimental and predicted main-ion toroidal rotation profiles during 1.0 and 1.7 MW ECH heating, where the rotation boundary conditions is taken from the experiment at $\rho = 0.8$ and neglecting numerical buffer regions. Good agreement between both the shape of the toroidal rotation, as well as the magnitude of the toroidal rotation variation across the profiles is accurately captured. Also included in Fig. 7 are profiles reconstructed with variation of the Prandtl number $Pr = 0.7 \pm 0.1$ incorporating reasonable ranges around the time-average $Pr = 0.7$ seen in the gyrokinetic simulations. A shorter time averaging period of the residual stress shown in Fig. 4 over $t(v_{th}/L_{Ti}) = 500 - 700$ is also presented showing that the resulting profile in insensitive to the range of time averaging used in the simulation. This clearly indicates that fluctuation-induced residual stress can generate intrinsic torque sufficiently strong to produce macroscopic changes in main-ion angular momentum. The conclusion is insensitive to the

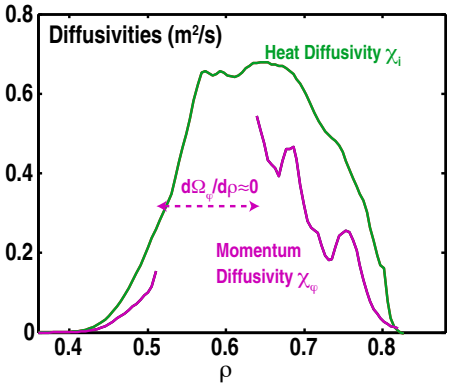

FIG. 5: Ion heat and momentum diffusivity used to validate $Pr \approx 0.7$. At the off-axis peak of the rotation profile $\partial\Omega_\varphi/\partial\rho$ is zero, and χ_φ is undefined

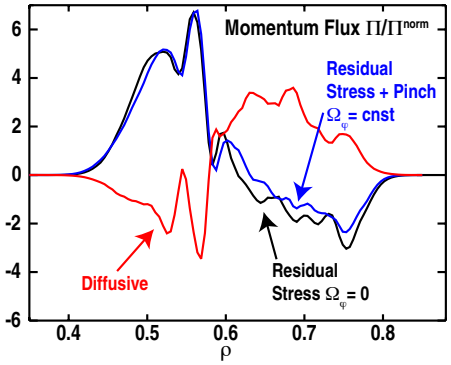

FIG. 6: Momentum flux from three simulations used to separate residual stress, momentum diffusion and pinch.

Prandtl number with reasonable ranges around $Pr = 0.7$. The level of agreement obtained represents a significant advancement in the validation of global nonlinear gyrokinetics to predict the angular momentum profiles.

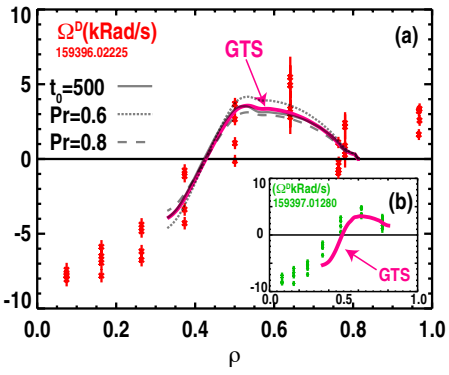

FIG. 7: Main-ion toroidal rotation and GTS simulation for (a) 1.0 and (b) 1.7 MW heating with experimental data taken from Fig. 1. In (a) we include the prediction including a later time average and Prandtl numbers within the variation of the GTS simulation.

Summary— Experiments on DIII-D have revealed that fluctuation-induced residual stress is capable of producing the experimentally observed intrinsic main-ion toroidal rotation in both shape and magnitude. Global nonlinear gyrokinetic simulations using the experimentally measured plasma profiles predict ITG turbulence and residual stress in the radial region where the toroidal rotation undergoes a strong change of gradient. Residual stress momentum flux that arises in the gyrokinetic simulations is balanced by turbulent momentum diffusion and the turbulent momentum pinch is found to be a small contributor to the momentum transport. Integrating the momentum balance equation produces a predicted main-ion toroidal velocity profile that agrees well with the experimental measurements, demonstrating that fluctuation-induced residual stress is capable of producing experimentally observed intrinsic rotation profiles.

* Electronic address: bgriers@pppl.gov; This material is based upon work supported by the U.S. Department of Energy, Office of Science, Office of Fusion Energy Sciences, using the DIII-D National Fusion Facility, a DOE Office of Science user facility under awards, DE-AC02-09CH11466[1], DE-FC02-04ER54698[2], and DE-FG07-07ER54917[3]. DIII-D data shown in this paper can be obtained in digital format by following the links at https://fusion.gat.com/global.D3D_DMP.

[1] M. P. Baldwin, P. B. Rhines, H. P. Huang, and M. E. McIntyre, Science (2007).
[2] A. C. Boxer, *et. al.*, Nature Physics **6**, 207 (2010).
[3] K. Ida and J. E. Rice, Nuclear Fusion **54**, 045001 (2014).
[4] J. Rice, *et. al.*, Physical Review Letters (2011).
[5] A. Bortolon, B. P. Duval, A. Pochelon, and A. Scarabosio, Physical Review Letters **97**, 1 (2006).
[6] C. L. Fiore, D. R. Ernst, Y. A. Podplay, D. Mikkelsen, and N. T. Howard, Physics of Plasmas **19**, 056113 (2012).
[7] J. W. Berkery, *et. al.*, Physical Review Letters **104**, 035003 (2010).
[8] W. X. Wang, *et. al.*, Physics of Plasmas **13**, 092505 (2006).
[9] J. E. Rice, Physics of Plasmas **19**, 056106 (2012).
[10] J. S. deGrassie, *et. al.*, Physics of Plasmas **11**, 4323 (2004).
[11] J. S. deGrassie, *et. al.*, Physics of Plasmas **14**, 056115 (2007).
[12] R. M. McDermott, *et. al.*, Nuclear Fusion **54**, 043009 (2014).
[13] A. E. White, *et. al.*, et al., Physics of Plasmas **20**, 056106 (2013).
[14] Y. J. Shi, *et. al.*, et al., Nuclear Fusion **53**, 113031 (2013).
[15] M. Barnes, *et. al.*, Physical Review Letters **111**, 055005 (2013).
[16] B. A. Grierson, *et. al.*, Review of Scientific Instruments **83**, 10D529 (2012).
[17] B. A. Grierson, *et. al.*, K. H. Burrell, Physics of Plasmas **19**, 056107 (2012).
[18] J. Luxon, Nuclear Fusion **42**, 614 (2002).
[19] A. G. Peeters, C. Angioni, and t. A. U. Team, Physics of Plasmas (1994-present) **12**, 072515 (2005).
[20] F. I. Parra, M. Barnes, and A. G. Peeters, Physics of Plasmas **18**, 062501 (2011).
[21] H. Sugama, *et. al.*, Plasma Physics and Controlled Fusion **53**, 024004 (2011).
[22] P. H. Diamond, *et. al.*, Nuclear Fusion **49**, 045002 (2009).
[23] F. I. Parra and M. Barnes, Plasma Physics and Controlled Fusion **57**, 045002 (2015).
[24] R. R. Dominguez and G. M. Staebler, Physics of Fluids B: Plasma Physics **5**, 3876 (1993).
[25] Ö. D. Gürcan, P. H. Diamond, T. S. Hahm, and R. Singh, Physics of Plasmas **14**, 042306 (2007).
[26] Y. Camenen, A. Bortolon, and B. P. Duval, Physical Review (2010).
[27] Ö. D. Gürcan, *et. al.*, Physics of Plasmas **17**, 112309 (2010).
[28] Y. Camenen, Y. Idomura, S. Jolliet, and A. G. Peeters, Nuclear Fusion **51**, 073039 (2011).
[29] Z. X. Lu, *et. al.*, Nuclear Fusion **55**, 093012 (2015).
[30] G. M. Staebler, J. E. Kinsey, and R. E. Waltz, Physics of Plasmas **12**, 102508 (2005).
[31] R. J. Hawryluk, Course on Physics of Plasmas Close to Thermonuclear Conditions pp. 1–28 (1979).
[32] W. X. Wang, *et. al.*, Physics of Plasmas **17**, 072511 (2010).
[33] W. M. Solomon, Nuclear Fusion **49**, 085505 (2009).
[34] N. Mattor and P. H. Diamond, Physics of Fluids **31**, 1180 (1988).
[35] F. J. Casson, *et. al.*, Physics of Plasmas **16**, 092303 (2009).